CrossMark

electronic reprint

JOURNAL OF APPLIED CRYSTALLOGRAPHY

ISSN: 1600-5767

journals.iucr.org/j

A computationally efficient method to solve the Takagi–Taupin equations for a large deformed crystal

Ari-Pekka Honkanen, Giulio Monaco and Simo Huotari

J. Appl. Cryst. (2016). **49**, 1284–1289

JOURNAL OF APPLIED CRYSTALLOGRAPHY
ISSN 1600-5767

A computationally efficient method to solve the Takagi–Taupin equations for a large deformed crystal

Ari-Pekka Honkanen,[a]* Giulio Monaco[b] and Simo Huotari[a]

[a]Department of Physics, PO Box 64, FI-00014 Helsinki, Finland, and [b]Physics Department, University of Trento, Via Sommarive 14, 38123 Povo (TN), Italy. *Correspondence e-mail: ari-pekka.honkanen@helsinki.fi

Received 27 January 2016
Accepted 27 June 2016

Edited by S. Boutet, SLAC National Accelerator Laboratory, Menlo Park, USA

Keywords: X-ray diffraction; Takagi–Taupin equations; deformed crystals.

A treatise is presented on solving the Takagi–Taupin equations in the case of a strain field with an additional, spatially slowly varying component (owing to, for example, heat expansion or angular compression). It is shown that such a component typically has a negligible effect on the shape of the reflectivity curve when considering the reflectivity of a microscopic surface area of the crystal. However, it makes the centroid of that curve shift in terms of the wavelength (or the incidence angle) as a function of the position of the mentioned area, which alters the shape of the overall reflectivity curve integrated over the crystal's macroscopic surface. The validity of the method is demonstrated by comparing computed reflectivity curves with experimental ones for bent silicon wafers. A good agreement is observed.

1. Introduction

In the hard X-ray regime, the X-ray spectrometers with the highest energy resolution are nowadays based on diffractive crystal optics. In the sub-eV energy resolution range, bent crystals are often used to yield an optimal collection solid angle and a suitable bandwidth. There are numerous different curved crystal geometries in common use, such as the Johann, Johansson and von Hamos geometries (Johann, 1931; Johansson, 1932; von Hamos, 1932). X-ray crystal spectrometers based on such designs are installed at various synchrotron light sources worldwide (*e.g.* Itou *et al.*, 2001; Fister *et al.*, 2006; Verbeni *et al.*, 2009; Hiraoka *et al.*, 2013; Sokaras *et al.*, 2013; Alonso-Mori *et al.*, 2015; Rueff *et al.*, 2015).

To design the most precise instruments, one requires a solid theoretical knowledge of the diffraction properties of crystals. To this end, highly relevant for bent crystals is the theory of dynamical X-ray diffraction in deformed crystals that was developed independently by S. Takagi and D. Taupin (Takagi, 1962, 1969; Taupin, 1964). At the heart of the theory are the so-called Takagi–Taupin (TT) equations, which describe the wavefield in a (quasi)periodic medium. For the usual case of two-beam diffraction, one obtains the X-ray reflectivity curve of a crystal by solving a pair of partial differential equations. When the strain field is solely depth dependent, these equations reduce to one ordinary differential equation. This is the usual approach to modelling the X-ray reflectivity of bent crystals, but it is not enough, for example, for spherically bent crystals used in Johann-type spectrometers, owing to a spatially slowly changing component of strain arising from so-called angular compression (Verbeni *et al.*, 2009; Honkanen *et al.*, 2014*a*,*b*). Accurate numerical methods have been developed (Authier *et al.*, 1968; Yan & Li, 2014), yet solving

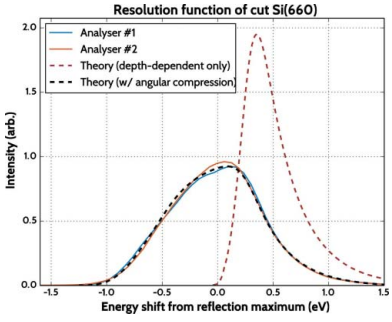

the general two-beam TT equations for a crystal wafer of a typical size of ~100 mm is a computational challenge. Another important example of the situations that require solution of the TT equations over a large crystal area is X-ray monochromators with heat-load-induced deformations (Hoszowska *et al.*, 2001; Zhang *et al.*, 2013).

In this paper, we examine the solutions of the TT equations and as a result present an efficient method for computing the reflectivity curve of a large deformed crystal. The method applies to strain fields that can be decomposed into a sum of a depth-dependent component that varies rapidly along the path of the incident and the diffracted beams and a slowly changing component that varies on the macroscopic scale. The result generalizes our earlier procedure presented by Honkanen *et al.* (2014*b*).

2. TT equations with a slowly changing strain component

The Takagi–Taupin equations that describe two-beam diffraction in a crystal are (Gronkowski, 1991)

$$\begin{cases} \dfrac{\partial D_0}{\partial s_0} = -\pi i k \chi_0 D_0 - \pi i k C \chi_{\bar{h}} D_h \\ \dfrac{\partial D_h}{\partial s_h} = -\pi i k C \chi_h D_0 + 2\pi i k \beta_h D_h \end{cases} \quad (1)$$

where D_0 and D_h are the amplitudes of the incident and diffracted waves inside the crystal, $\partial/\partial s_0$ and $\partial/\partial s_h$ are derivatives with respect to the directions of the forward diffracted and diffracted waves, k is the wavenumber of the incident wave, χ_0 and χ_h are the Fourier components of the susceptibility corresponding to reciprocal lattice vectors $\mathbf{0}$ and $\mathbf{h}$, and C is the polarization factor. β_h is given by

$$\beta_h = \frac{1}{2}\left[\frac{|\mathbf{k}+\mathbf{h}-\nabla(\mathbf{u}\cdot\mathbf{h})|^2 - k^2}{k^2} - \chi_0\right] \quad (2)$$

$$= \frac{|\mathbf{h}|^2}{2k^2} + \frac{\mathbf{k}\cdot\mathbf{h}}{k^2} - \frac{\chi_0}{2} - \frac{1}{k}\frac{\partial(\mathbf{u}\cdot\mathbf{h})}{\partial s_h}, \quad (3)$$

where $\mathbf{k}$ is the wavevector of the incident wave and $\mathbf{u}$ is the displacement field. The reflectivity curve of an arbitrarily deformed crystal is obtained by varying either the direction or the length of $\mathbf{k}$ and solving the TT equations in the vicinity of the Bragg condition.

For solving the TT equations, β_h is typically reformulated in terms of the Bragg angle and the angular deviation from the Bragg condition. However, as the Bragg angle is not defined for wavelengths smaller than the backscattering wavelength, this formulation ceases to be valid in near-backscattering conditions (Caticha & Caticha-Ellis, 1982). In this paper, we circumvent the arising problems by formulating (3) in terms of the wavelength λ and the incidence angle θ so that

$$\beta_h = \frac{\lambda^2}{2d_h^2} - \frac{\lambda}{d_h}\sin\theta - \frac{\chi_0}{2} - \lambda\frac{\partial(\mathbf{u}\cdot\mathbf{h})}{\partial s_h}, \quad (4)$$

where d_h stands for the separation of the diffractive Bragg planes.

As one can see, the effect of the strain field comes into the TT equations *via* parameter β_h. Thus, the radiation propagation is identical in crystals with different strain fields if the β_h parameters are exactly alike. One can tune the value of β_h by changing the angle of incidence θ or the wavelength λ of the radiation. This is approximately true even in the latter case, even if a change of λ affects the solutions of equations (1) in a nontrivial way, since the relative shift of λ owing to the strain is practically negligible.

Let us consider the diffraction of a crystal in two different cases. In the first case the displacement field is $\mathbf{u}_\mathrm{I} = \mathbf{u}_\mathrm{f}(z)$, which accounts for a rapid displacement of the depth-dependent strain. In the other case the displacement field is $\mathbf{u}_\mathrm{II} = \mathbf{u}_\mathrm{f} + \mathbf{u}_\mathrm{s}$, where the component of the strain described by $\mathbf{u}_\mathrm{s} = \mathbf{u}_\mathrm{s}(x, y)$ is nearly linear in terms of s_h on the microscopic scale, thus representing the slowly varying component of the strain. The coordinate system is chosen so that the $\mathbf{z}$ direction is normal to the crystal surface, the positive direction being outward from the crystal. The strain field of a spherically bent crystal analyser serves as an example of the latter kind of displacement field (Honkanen *et al.*, 2014*b*). Subscripts I and II, respectively, will be used throughout the article to refer to the quantities relating to the diffraction of these cases. Substituting $\mathbf{u}_\mathrm{I}$ and $\mathbf{u}_\mathrm{II}$ into (4) and taking their difference, we get

$$\Delta\beta_h = \frac{\lambda_\mathrm{II}^2 - \lambda_\mathrm{I}^2}{2d_h^2} - \left(\frac{\lambda_\mathrm{II}}{d_h}\sin\theta_\mathrm{II} - \frac{\lambda_\mathrm{I}}{d_h}\sin\theta_\mathrm{I}\right) - \lambda_\mathrm{II}\frac{\partial(\mathbf{u}_\mathrm{s}\cdot\mathbf{h})}{\partial s_h} - (\lambda_\mathrm{II} - \lambda_\mathrm{I})\frac{\partial(\mathbf{u}_\mathrm{f}\cdot\mathbf{h})}{\partial s_h}. \quad (5)$$

On the basis of the earlier argument, the solution to the TT equation is found to be equivalent in both cases if the similarity condition $\Delta\beta_h = 0$ holds. In the following, we show that the condition is met *via* a constant change in the incidence angle or wavelength under certain assumptions. The two cases are examined separately and the results are applied to compute the reflectivity curves.

2.1. Scanning the incident wavelength

Let us first examine the case of a varying wavelength. We denote the difference of wavelengths between cases I and II with $\delta\lambda \equiv \lambda_\mathrm{II} - \lambda_\mathrm{I}$. In this case the angle of incidence is kept constant, *i.e.* $\theta_\mathrm{I} = \theta_\mathrm{II} \equiv \theta$.

Since the differences caused by $\mathbf{u}_\mathrm{s}$ are small, we can make the first-order approximation

$$\lambda_\mathrm{II}^2 \simeq \lambda_\mathrm{I}^2 + 2\lambda_I\delta\lambda. \quad (6)$$

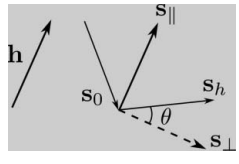

Figure 1
Relations of $\mathbf{s}_0$, $\mathbf{s}_h$, $\mathbf{s}_\parallel$, $\mathbf{s}_\perp$ and $\mathbf{h}$ to each other.

Thus the similarity condition can be written as

$$\frac{\lambda_I \delta\lambda}{d_h^2} - \frac{\delta\lambda}{d_h}\sin\theta - \lambda_I \frac{\partial(\mathbf{u}_s \cdot \mathbf{h})}{\partial s_h} - \delta\lambda \frac{\partial(\mathbf{u}_{II} \cdot \mathbf{h})}{\partial s_h} = 0. \quad (7)$$

We define a new basis with vectors $\mathbf{s}_\parallel$ and $\mathbf{s}_\perp$, respectively, parallel and perpendicular to $\mathbf{h}$, as shown in Fig. 1. The first partial derivative in (7) can now be written as

$$\frac{\partial(\mathbf{u}_s \cdot \mathbf{h})}{\partial s_h} = \frac{\varepsilon \sin\theta + \tau\cos\theta}{d_h}, \quad (8)$$

where $\varepsilon \equiv \partial(\mathbf{u}_s \cdot \hat{\mathbf{h}})/\partial s_\parallel$ is the normal strain in the direction of $\mathbf{h}$ and $\tau \equiv \partial(\mathbf{u}_s \cdot \hat{\mathbf{h}})/\partial s_\perp$ is the shear strain in the $\mathbf{s}_\parallel$–$\mathbf{s}_\perp$ plane. Substituting the former into (7) and neglecting $\delta\lambda\partial(\mathbf{u}_{II} \cdot \mathbf{h})/\partial s_h$ as second order, we get

$$\left(\frac{1}{d_h} - \frac{\sin\theta}{\lambda_I}\right)\delta\lambda - \varepsilon\sin\theta - \tau\cos\theta = 0. \quad (9)$$

Since the diffraction takes place in the vicinity of the Bragg condition, we can use Bragg's law to express d_h with high accuracy in terms of λ_I and θ_I:

$$d_h = \frac{\lambda_I}{2\sin\theta}. \quad (10)$$

Substituting the former into (9), the similarity condition becomes

$$\delta\lambda/\lambda_I = \varepsilon + \tau\cot\theta. \quad (11)$$

Notably in the case of exact backscattering or when $\tau = 0$ this reduces to the result expected from Bragg's law that was used by Honkanen *et al.* (2014*b*).

From equation (11) we now see that the change of the wavelength shift $\Delta(\delta\lambda)$ relative to the width of the diffraction peak $\Delta\lambda_I$ is

$$\Delta(\delta\lambda)/\Delta\lambda_I = \varepsilon + \tau\cot\theta, \quad (12)$$

which is typically $\lesssim 10^{-4}$ supposing we are not close to grazing-incidence conditions. This means that the effect of the additional strain components ε and τ present in case II can be accounted for by simply shifting the reflectivity curve of case I in the wavelength domain by an amount dictated by equation (11).

The validity of the derivation was studied using a one-dimensional TT solver implemented in Python/SciPy. The solver is freely available under MIT license at https://github.com/aripekka/pytakagitaupin. The derivation of the depth-dependent equation was according to Gronkowski (1991), with the exception of using (4) as the form of β_h in the derivation. The reflectivity curve for the symmetric 660 reflection of silicon was computed at incidence angles of 85, 75, 65 and 55° (approximate photon energies of 9.72, 10.02, 10.68 and 11.82 keV, respectively) for a set of constant strains ε varying from 0 to 10^{-3}. τ was set to zero. The thickness of the crystal was set to 3 mm in order to get rid of the thickness-related oscillations in the reflectivity curve which interfere with the accurate determination of the curve width. The shift of the reflectivity maximum and FWHMs as a function of ε were computed and the results were compared with the theoretical predictions of equations (11) and (12).

The relative shift in the wavelength as a function of strain ε is presented in Fig. 2, with the theoretical prediction. As one can see, the predicted shift is found to be in good accordance with the simulations and follows the behaviour expected simply from Bragg's law. The shape and the width of the reflectivity curve have a much weaker dependence on the strain, as shown in Fig. 3 for the FWHM. As in the case of the wavelength shift, the simulated results are found to follow the theoretical result.

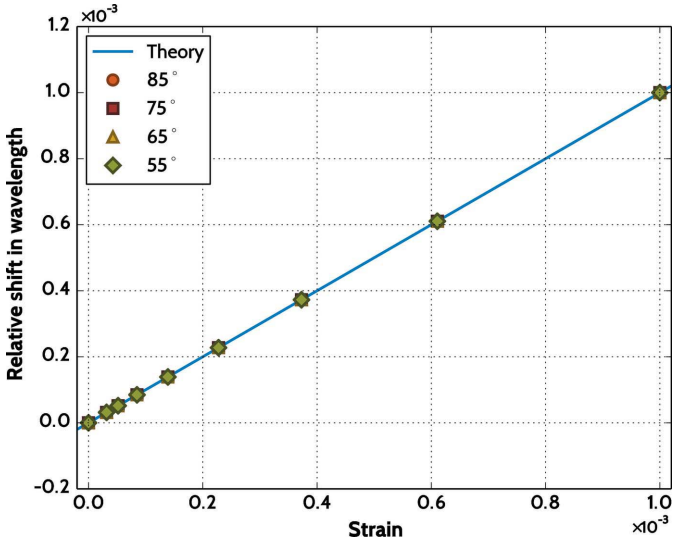

Figure 2
Simulated and theoretical shifts in the wavelength as a function of strain component ε at different incidence angles for the symmetrical Si(660) reflection. Some of the data points are not visible owing to their overlap.

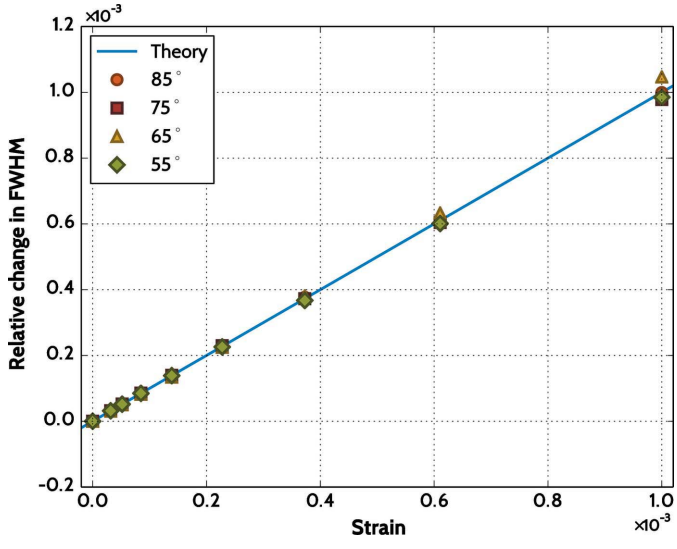

Figure 3
Simulated and theoretical changes in the FWHM of the reflectivity curve as a function of strain component ε at different incidence angles for the symmetrical Si(660) reflection. Some of the data points are not visible owing to their overlap.

2.2. Scanning the incidence angle

Another approach is offered by a variation of the beam's angle of incidence with respect to the crystal surface. We denote the difference of incidence angles between cases I and II by $\delta\theta \equiv \theta_{\rm II} - \theta_{\rm I}$. In this case the wavelength is kept constant, *i.e.* $\lambda_{\rm I} = \lambda_{\rm II} \equiv \lambda$. From equation (5), the similarity condition now becomes

$$\frac{1}{d_h}(\sin\theta_{\rm II} - \sin\theta_{\rm I}) + \frac{\partial(\mathbf{u}_s \cdot \mathbf{h})}{\partial s_h} = 0. \quad (13)$$

Acknowledging that the angles in equation (8) correspond to case II, we obtain by substitution

$$\sin\theta_{\rm II} - \sin\theta_{\rm I} + \varepsilon\sin\theta_{\rm II} + \tau\cos\theta_{\rm II} = 0. \quad (14)$$

By making the Taylor expansion in terms of $\delta\theta$ and retaining only the first-order terms we obtain for the similarity condition

$$\delta\theta = -\varepsilon\tan\theta_{\rm I} - \tau. \quad (15)$$

The change in the incidence angle shift $\Delta(\delta\theta)$ relative to the angular width of the diffraction $\Delta\theta_{\rm I}$ is found by differentiation of equation (15):

$$\frac{\Delta(\delta\theta)}{\Delta\theta_{\rm I}} = -\frac{\varepsilon}{\cos^2\theta_{\rm I}}. \quad (16)$$

As seen in the case of wavelength, the shift in the angle of incidence is again found to be linear in terms of the strain components ε and τ. However, in this case the first-order expressions diverge when $\theta = 90^\circ$. In addition, since (16) grows faster than (15) when θ approaches 90°, the change in the width of the rocking curve can not be necessarily neglected. In the vicinity of backscattering, one should consider a higher-order expansion of equation (14) in terms of $\delta\theta$. This is, however, out of the scope of this work as the situation becomes more complicated owing to the symmetry of the reflection at angles above 90°.

The validity of the derivation was examined using the one-dimensional TT solver as for the wavelength. The Si(660) reflection was studied at photon energies of 9.72, 10.02, 10.68 and 11.82 keV, corresponding approximately to the incidence angles of 85, 75, 65 and 55°, respectively. The constant strain component ε was varied from 0 to 10^{-3} and τ was set to zero.

The results are presented in Figs. 4 and 5. As in the case of wavelength, the simulated $\delta\theta$ follow the theoretical prediction (15) with high precision and the general shape of the curve appears to be independent of ε. Also, the FWHMs of the rocking curves are in good accordance with equation (15). At a higher Bragg angle at 9.72 keV, the simulated values begin to deviate from the theory as $\varepsilon\tan\theta_{\rm I}$ and $\varepsilon\cos^2\theta_{\rm I}$ become larger. Apart from the nonlinear regime, the theory holds well for the smaller values of ε.

3. Efficient computation of the reflectivity curves

From the results of the previous section, the effect of a slowly changing strain field can be taken into account locally by a simple shift of the solution to the TT equations on either the wavelength or the incidence angle scales. The width of the curve is also altered slightly, but as the relative change is expected to be <1%, it can be neglected in most cases. The reflectivity curve of the whole crystal is then obtained by summing the reflectivities of infinitesimal areas over the crystal surface. Since solving the TT equations can be computationally demanding for a macroscopic crystal, the derived results offer an intriguing method of computation in cases where a suitable strain component is present.

The reflectivity curve of a macroscopic crystal can be solved as follows. The TT equations (1) are solved in their one-

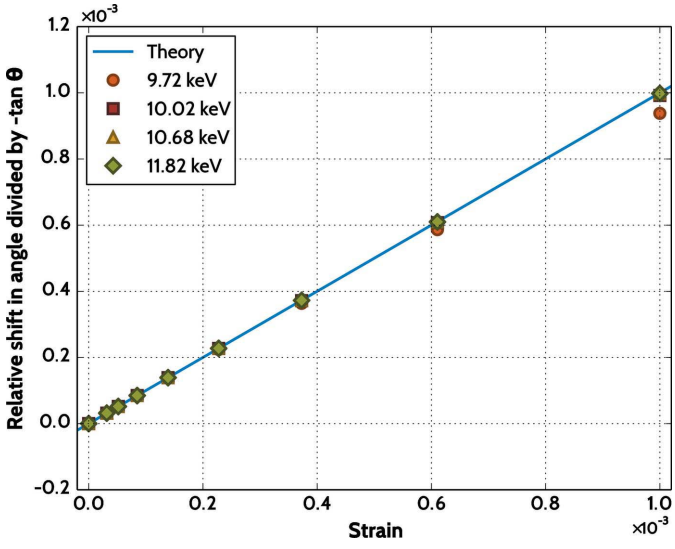

Figure 4
Simulated and theoretical shifts in the incidence angle as a function of strain component ε for different photon energies for the symmetrical Si(660) reflection. The data are divided by $-\tan\theta$ for clarity. Some of the data points are not visible owing to their overlap.

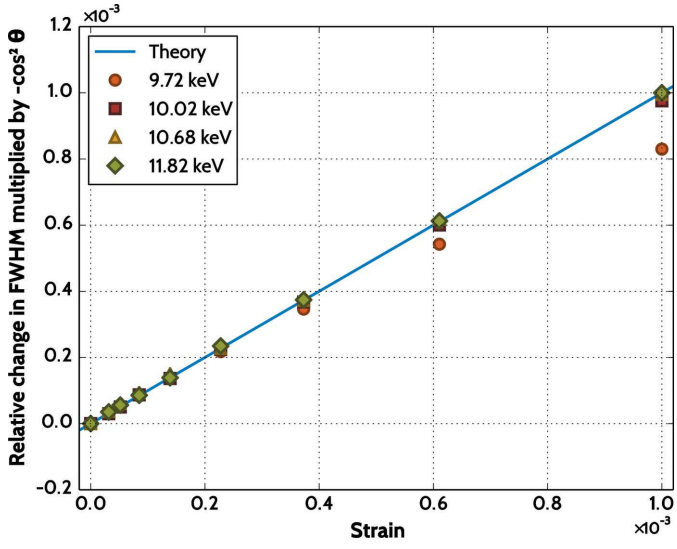

Figure 5
Simulated and theoretical changes in the FWHM of the rocking curve as a function of strain component ε for different photon energies for the symmetrical Si(660) reflection. The data are multiplied by $-\cos^2\theta$ for clarity. Some of the data points are not visible owing to their overlap.

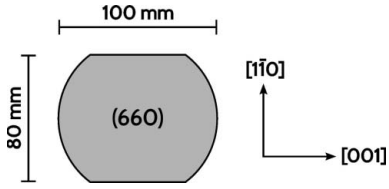

Figure 6
Geometry of the studied Si(660) analysers. 300 μm thick silicon wafers with a diameter of 100 mm were anodically bonded on a concave spherical glass surface. The bending radius was 1 m. Two cuts were made symmetrically along the [001] direction, limiting the analyser dimension in the [1$\bar{1}$0] direction to 80 mm.

dimensional form for the depth-dependent displacement component $\mathbf{u}_f$ as a function of θ or λ. The slowly changing component $\mathbf{u}_s$ is used to compute the $\delta\lambda$ or $\delta\theta$ distribution over the crystal surface using equation (11) or equation (15), respectively. The reflectivity curve of the crystal is then obtained by convolving the TT curve with the $\delta\lambda$ or $\delta\theta$ distribution. Other contributions, such as the bandwidth of the X-rays or geometric factors, are convolved with the result as needed.

4. Experimental verification

We applied the method to compute the reflectivity curve of an anodically bonded spherically bent Si(660) analyser with the geometry presented in Fig. 6 at an incidence angle of 88.7°. The bending radius of the crystals was 1 m and the thickness of the wafers was 300 m. The strain field of the wafer was calculated according to Honkanen *et al.* (2014*b*). The $\delta\lambda$ distribution was computed using equation (11), omitting the term containing τ as we are close to backscattering. The depth-dependent TT curve was convolved with the $\delta\lambda$ distribution and a Gaussian with an FWHM of 235 meV to take into account the bandwidth of the incident radiation in the experimental setup. We compared the theoretical prediction with the experimental curves of two such analysers measured at the inelastic X-ray scattering beamline ID20 at the ESRF. The details of the experimental setup are presented by Honkanen *et al.* (2014*a*).

The comparison between the theory and the experiment is presented in Fig. 7. The intensities of the curves are normalized with respect to the integrated intensity. The horizontal axis is the energy difference between the incident photon energy and the centroid of the measured reflectivity curve.[1] As it is seen, a good agreement is found between the theory and the experiment. For comparison, the red dashed curve shows the predicted reflectivity when the slowly changing strain component owing to angular compression is neglected. It is evident that the slowly changing component changes the shape of the curve to such an extent that it cannot be simply overlooked in the case of a macroscopic analyser crystal. It has a tendency to increase the spectral weight at the energy gain

[1] The absolute energy can in principle be determined as well, but as we concentrate on the use of the method in energy-loss spectroscopies, the relative changes on the energy shift axis are more relevant.

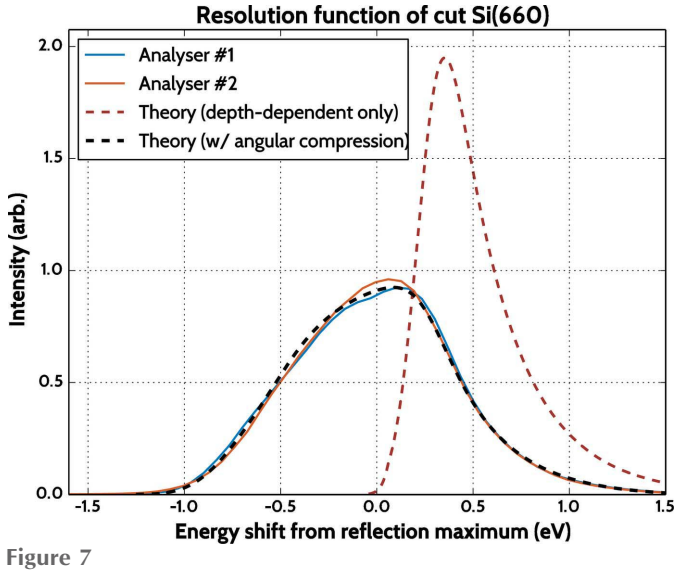

Figure 7
The measured reflectivity curves of two cut Si(660) analysers (solid lines) compared with the theoretical prediction (black dashed line). The red dashed line shows the predicted reflectivity in the case where the slowly changing strain component is not taken into account.

side (negative energy shift) of the spectrum, and hence creates an apparent shift of the reflectivity curve in this example by ∼0.5 eV.

5. Conclusions

In this paper we have examined how solutions of TT equations behave in the presence of a slowly varying component of the strain field. We applied the results to construct an efficient semi-analytical method to compute the X-ray reflectivity of deformed crystal with a slowly varying strain component.

We used the method to compute the reflectivity curve of an Si(660) analyser cut in a specific way. When this curve is compared with the measured reflectivity curves, a precise correspondence is found. Such an agreement found in the case of the examined nontrivial geometry speaks for the predictive power of the presented method, which offers an appealing alternative for effective computation of the reflectivity curves of large deformed crystals.

Acknowledgements

The authors would like to thank Roberto Verbeni, Laura Simonelli, Marco Moretti Sala, Ali Al-Zein and Michael Krisch for the experimental data of the bent silicon analysers. APH and SH were funded by the Academy of Finland (grants 1254065, 1283136 and 1259526).

References

Alonso-Mori, R., Sokaras, D., Zhu, D., Kroll, T., Chollet, M., Feng, Y., Glownia, J. M., Kern, J., Lemke, H. T., Nordlund, D., Robert, A., Sikorski, M., Song, S., Weng, T.-C. & Bergmann, U. (2015). *J. Synchrotron Rad.* **22**, 612–620.
Authier, A., Malgrange, C. & Tournarie, M. (1968). *Acta Cryst.* A**24**, 126–136.

Caticha, A. & Caticha-Ellis, S. (1982). *Phys. Rev. B*, **25**, 971–983.
Fister, T. T., Seidler, G. T., Wharton, L., Battle, A. R., Ellis, T. B., Cross, J. O., Macrander, A. T., Elam, W. T., Tyson, T. A. & Qian, Q. (2006). *Rev. Sci. Instrum.* **77**, 063901.
Gronkowski, J. (1991). *Phys. Rep.* **206**, 1–41.
Hamos, L. von (1932). *Naturwissenschaften*, **20**, 705–706.
Hiraoka, N., Fukui, H., Tanida, H., Toyokawa, H., Cai, Y. Q. & Tsuei, K. D. (2013). *J. Synchrotron Rad.* **20**, 266–271.
Honkanen, A.-P., Verbeni, R., Simonelli, L., Moretti Sala, M., Al-Zein, A., Krisch, M., Monaco, G. & Huotari, S. (2014*a*). *J. Synchrotron Rad.* **21**, 762–767.
Honkanen, A.-P., Verbeni, R., Simonelli, L., Moretti Sala, M., Monaco, G. & Huotari, S. (2014*b*). *J. Synchrotron Rad.* **21**, 104–110.
Hoszowska, J., Mocella, V., Zhang, L., Migliore, J.-S., Freund, A. K. & Ferrero, C. (2001). *Nucl. Instrum. Methods Phys. Res. Sect. A*, **467–468**, 631–634.
Itou, M., Hiraoka, N., Ohata, T., Mizumaki, M., Deb, A., Sakurai, Y. & Sakai, N. (2001). *Nucl. Instrum. Methods Phys. Res. Sect. A*, **467–468**, 1109–1112.
Johann, H. H. (1931). *Z. Phys.* **69**, 185–206.
Johansson, T. (1932). *Sci. Nat.* **20**, 758–759.
Rueff, J.-P., Ablett, J. M., Céolin, D., Prieur, D., Moreno, T., Balédent, V., Lassalle-Kaiser, B., Rault, J. E., Simon, M. & Shukla, A. (2015). *J. Synchrotron Rad.* **22**, 175–179.
Sokaras, D., Weng, T.-C., Nordlund, D., Alonso-Mori, R., Velikov, P., Wenger, D., Garachtchenko, A., George, M., Borzenets, V., Johnson, B., Rabedeau, T. & Bergmann, U. (2013). *Rev. Sci. Instrum.* **84**, 053102.
Takagi, S. (1962). *Acta Cryst.* **15**, 1311–1312.
Takagi, S. (1969). *J. Phys. Soc. Jpn*, **26**, 1239–1253.
Taupin, D. (1964). *Bull. Soc. Fr. Miner. Crist.* **87**, 469–511.
Verbeni, R., Pylkkänen, T., Huotari, S., Simonelli, L., Vankó, G., Martel, K., Henriquet, C. & Monaco, G. (2009). *J. Synchrotron Rad.* **16**, 469–476.
Yan, H. & Li, L. (2014). *Phys. Rev. B*, **89**, 014104.
Zhang, L., Sánchez del Río, M., Monaco, G., Detlefs, C., Roth, T., Chumakov, A. I. & Glatzel, P. (2013). *J. Synchrotron Rad.* **20**, 567–580.